Chapter 2 : Literature Review

This chapter contains a critical review of the existing literature on the different methods for successful welding of similar and dissimilar titanium alloys. It also includes discussion on the microstructure development, challenges that occurred and weld characteristics obtained using different welding methods for titanium alloys. Furthermore, a comprehensive review of the selection of welding processes for dissimilar titanium alloys has been done on the basis of the cost incurred and weld characteristics obtained with the different welding processes used for titanium alloys. The research gap obtained from the literature survey, problem formulation and objectives for experimental work have been discussed at the end of this chapter.

2.1 Microstructure development and phase evolution in titanium alloys

Microstructure development and phase evolution in titanium alloys are critical to their mechanical properties. Upon cooling, titanium alloys undergo phase transformations such as $\alpha \rightarrow \beta$ in the β region and $\beta \rightarrow \alpha + \beta$ in the α+β region. These transformations affect grain size, phase composition, and mechanical behaviour. Factors like alloy composition, cooling rate, and heat treatment influence microstructure evolution, determining the presence of phases like α, β, α', and α''. Understanding these processes is essential for tailoring titanium alloys' properties for specific applications, such as aerospace components, biomedical implants, and high-performance engineering materials [3, 29].

2.1.1 Classification of the titanium alloys

As discussed in Section 1.1.2, titanium alloys can be classified depending upon the amount of α and β phases present in the alloy and these phases can be altered by

adding α and β stabilizers. Figure 2.1 shows the pseudo-binary phase diagram, where depending upon compositions of β stabilizers α, β, (α+β) and β alloys have been divided and some U.S.-based important alloys are marked [3]. The diagram clearly shows that alloys such as Ti-5Al-2.5Sn are α-alloys and Ti-8Al-1Mo-1V are near-α alloys that barely contain β-phase. Ti-6Al-4V falls in the α+β alloy region and has sufficient β-phase. However, alloys such as Ti-13V-11Cr-3Al are at the high end of the meta stable β-alloys and contain a large amount of β-phase, owing to slow transformation kinetics, and will remain β-phase on cooling to higher temperatures [3]. The M_s and M_f lines introduced in the diagram refer to martensitic transformation start and martensitic transformation finish lines during nonequilibrium cooling. These martensitic phases appear during the rapid cooling of (α+β) alloys, as in steel. Different martensitic phases have been discussed later in the chapter [29].

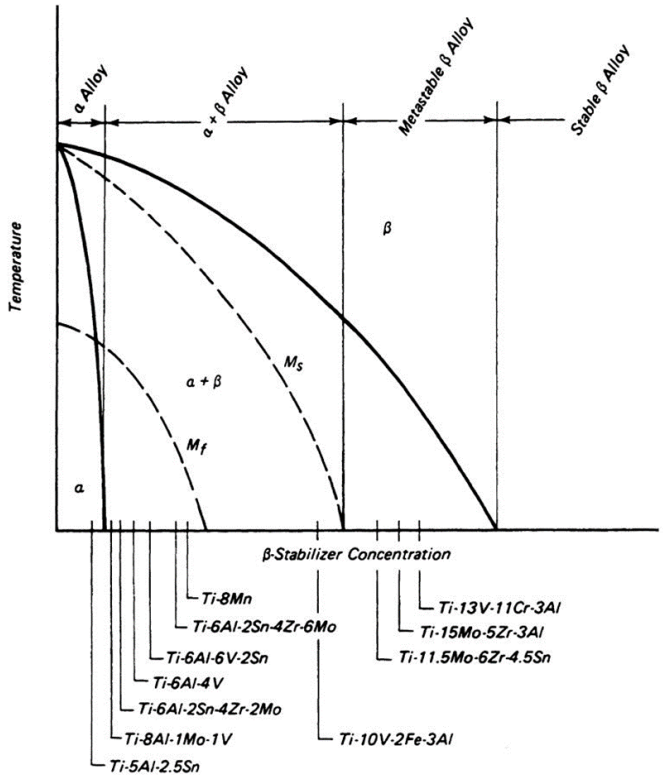

Figure 2.1 Classification of titanium alloys on pseudo-binary phase diagram of titanium [3]

Typical microstructure in α, α+β, and β alloys

The microstructures of different alloys show variations in the morphological development of the α and β phases. The variations are dependent on alloy chemistry, prior work, the temperature from which it was cooled, and the rate of cooling. Equiaxed, coarse and fine acicular microstructures can be produced by different processes. To keep the (α+β) alloy relatively soft and machinable, the alloy is heated to about 730 °C in the lower range of the (α+β) region, held for 4 hours, then furnace cooled to 25 °C [1]. This treatment, called mill annealing, produces a microstructure of globular crystals of β in an α matrix. Figure 2.2 shows the equiaxed morphology of CP-Ti (α-alloy) microstructure, globular particles of β-phase in the matrix of α-phase, Widmanstätten morphology in (α+β) alloy (Ti-6Al-4V), and equiaxed morphology in β-alloy (Ti-13V-11Cr-3Al), respectively [3]. The displayed microstructures are shown for representation but are certainly not all-inclusive, as the actual microstructure is influenced by both chemistry and processing methods. The details related to the development of different morphologies in the microstructure of titanium alloys will be discussed later in this chapter. Generally, α-alloys are not heat treatable, and their mechanical properties cannot change significantly through such methods. However, morphologies can be altered depending on the maximum temperature during cooling and the cooling rate. Sometimes, a fine acicular morphology developed in the α-alloys leads to little improvement in mechanical properties. However, (α+β) titanium alloys are considered heat treatable, and significant changes in mechanical properties can be achieved by altering the phase composition and morphology in the alloy. Therefore, in further sections, the development of different morphologies has been studied using (α+β) alloys [3, 17].

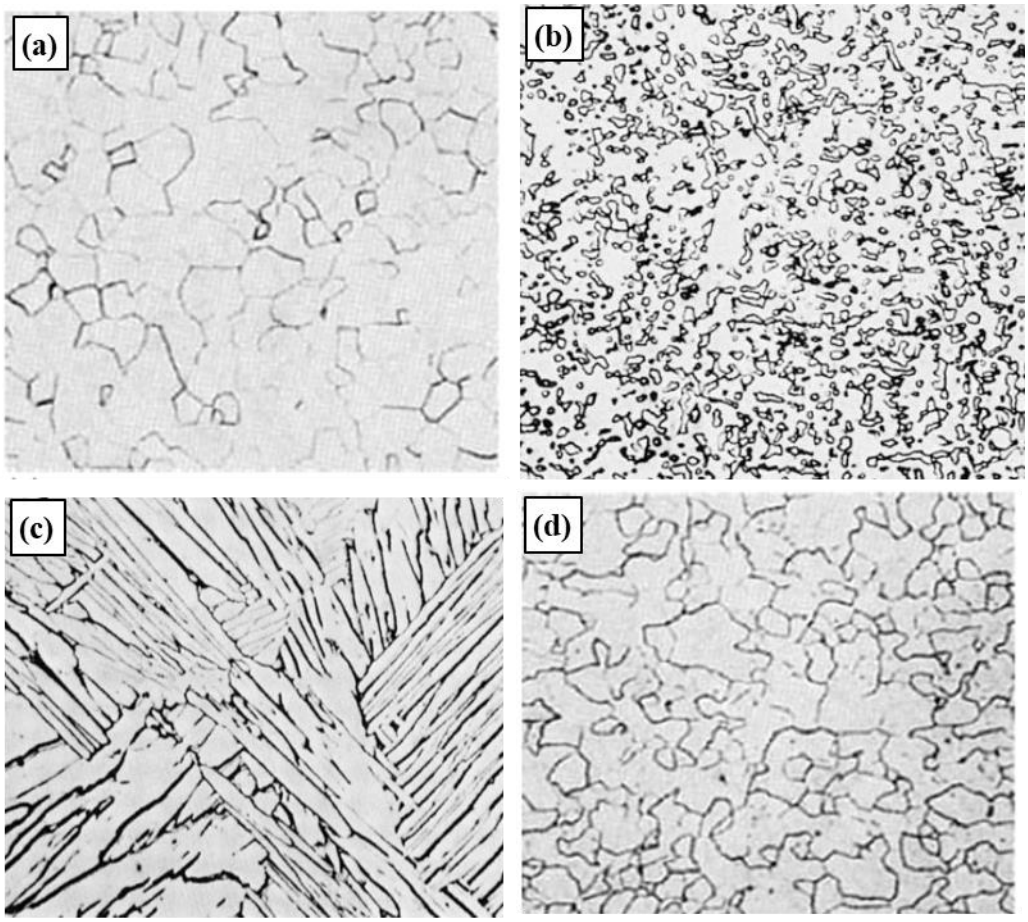

Figure 2.2 (a) Equiaxed α in unalloyed Ti (CP-Ti); (b) mill-annealed (α + β) alloy (Ti-6Al-4V) (c) Widmanstätten (α+β) alloy (Ti-6Al-4V); (d) equiaxed β in Ti-13V-11Cr-3Al [3]

2.1.2 Solid state phase transformation in (α+β) titanium alloys

The Widmanstätten morphology that develops in the (α+β) alloy upon slow cooling is shown in Figure 2.2 (c). The formation process, referred to as 'sympathetic nucleation and growth', is demonstrated schematically in Figure 2.3 [3, 7]. It uses a constant-composition phase diagram section at 6 wt.% Al to illustrate the formation of alpha upon cooling. When this (α+β) alloy is cooled above the β-transus temperature, the HCP α-phase starts to form as plates with a basal plane parallel to a special plane in the β-phase. The growth is fast along the plates in comparison to the perpendicular direction. The darker β phase is trapped between the brighter α plates. The microstructure consists of parallel α plates surrounded by the β phase. α plates

form parallel to one specific plane of β-phase and meet α plates formed on another plane of β-phase. A high-angle grain boundary exists between the α crystals and etches to reveal a line separating them [7]. The microstructural morphology, consisting of these sets of parallel plates that have formed with a crystallographic relationship to the phase from which they formed, is known as a Widmanstätten structure [30].

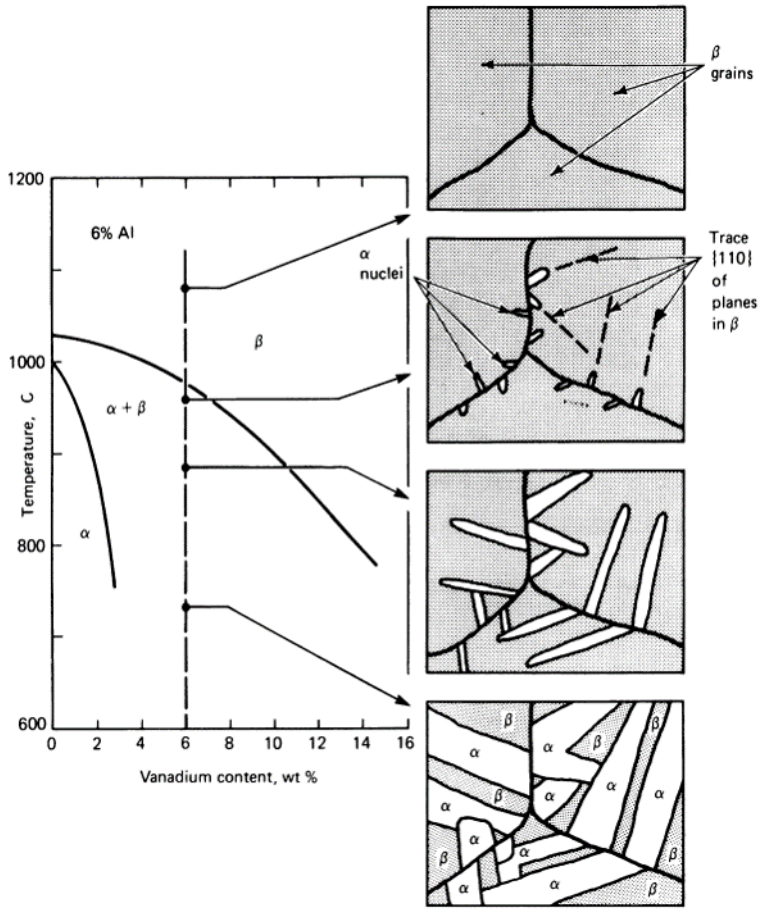

Figure 2.3 Development of a Widmanstätten morphology in an (α+β) alloy (Ti-6Al-4V) [3]

2.1.3 Typical cooling rates and phase transformations in the (α+β) alloy

Ahmed and Rack (1998) carried out the investigations to understand the influence of rapid cooling on the microstructure of the Ti-6Al-4V alloy by, using a modified Jominy end quench test method from the β-phase [29]. The resultant morphologies developed with different cooling rates are shown using a schematic continuous

cooling diagram for Ti-6Al-4V in Figure 2.4, and the corresponding values are tabulated in Table 2.1. The formation of a fully martensitic microstructure has been observed at cooling rates above 410 °C/s. A massive transformation (mixed microstructures of martensitic α', transformed α and various morphological forms of diffusion controlled α) was observed at a cooling rate between 410 and 20 °C/s, and this transformation is slowly replaced by the diffusion-controlled Widmanstätten α phase at lower cooling rates (< 20 °C/s) [29, 30].

Welding imposes a high rate of heating and cooling thermal cycle on the material. At higher cooling rates, the driving force is increased, and nucleation of the α phase not only occurs on grain boundaries but also from existing α plates in the grain interior. As a result, within the remaining β phase, basketweave Widmanstätten α (shown in Figure 2.2 (c)) forms in a pseudo-random fashion. This microstructural morphology, consisting of thinner α plates within the colonies, is designated as a “basket weave” Widmanstätten structure [31]. Typical cooling rates in some important welding processes are mentioned in the Table 2.2 [29].

Table 2.1 Different welding processes and their cooling rates [29]

Welding processes	**Typical cooling rate**
Laser beam, Electron beam, and Resistance welding (Low heat input processes)	100 - 10000°C/s
Friction stir welding	50 - 150°C/s)
Gas-tungsten, Gas-metal, or Plasma arc welding	10 - 100°C/s

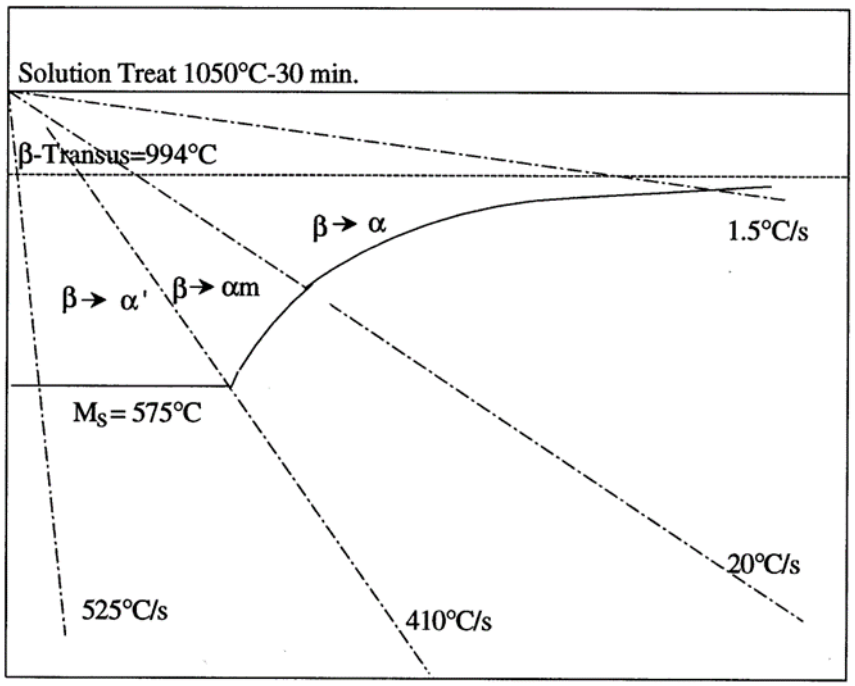

Figure 2.4 Schematic continuous cooling diagram for Ti–6Al–4V [29]

Table 2.2 Phase change with respect to different type of transformations [5, 29]

Cooling Rate (°C/s)	Type of transformation	Phase change and morphology
CR > 410	Rapid (Diffusion less)	β → α', α'' Acicular morphology
20 < CR < 410	Moderately fast (Mixed)	β → α_m (α, α') Mixed morphology
CR < 20	Diffusional control or slow	β → α Widmanstätten morphology or Allotriomorphic (grain boundary α)

The metastable phases (α', α'')

The physical and mechanical properties of Ti-6Al-4V are significantly influenced by the presence of metastable phases formed during rapid cooling. These metastable phases are referred to as the martensite of phases of titanium alloys. One such phase is α', which has an HCP structure and, due to its rapid nucleation and growth, contains a higher dislocation density compared to the primary α grains. It is obtained

by quenching from above 900 °C, and it has an acicular or sometimes fine-lamellar microstructure [29]. Therefore, the deformation mechanisms in α' are similar to those in α, with the main difference being a higher dislocation density in the undeformed state and a smaller plate thickness. Both the smaller grain size and the higher dislocation density suggest that α' is harder than α. Additionally, this phase can undergo more strain hardening than the α phase. Another metastable phase in Ti-6Al-4V is α", which has a rhombic structure instead of hexagonal [4]. It is a relatively soft martensite that forms during the quenching of the beta phase with 10 ± 2 wt.% vanadium, at temperatures between 750 and 900 °C. The α" martensite can also form as a stress-induced product by straining metastable beta. This phase can be considered an intermediate between HCP and BCC, with mechanical properties close to those of the β phase [32].

The intermetallic phase (α_2)

During heating of Ti-6Al-4V above 500 °C, alloy element partitioning takes place, leaving a larger percentage fraction of elements like Al, O, and Sn available for enriching the α phase. This leads to the precipitation of coherent Ti_3Al particles, also known as the α_2 phase. These particles can be sheared by dislocations and can also experience an extensive pileup of dislocations against boundaries [33]. Ti_3Al particles grow in an ellipsoidal shape, with their long axis parallel to the hexagonal lattice's c-axis. The presence of O and Sn can further enhance the precipitation of this intermetallic phase [30].

2.1.4 Effect of different cooling rates on microstructure of (α+β) alloy

Upon cooling rapidly, beta may decompose by a martensite reaction, similar to that for pure titanium, and form a Widmanstätten pattern. The structure present after

quenching at 25 °C depends on the annealing temperature. Different types of martensite can form, depending on the alloy chemistry and the quenching temperature. Upon quenching from above the β transus, the structure is all martensitic α' and α" with a small amount of β (although in some alloys the retained-β has not been observed) [3, 29].

Ti-6Al-4V is one of the most widely used (α+β) titanium alloys, containing 6 wt.% Al and 4 wt.% V. The properties of this alloy are developed by relying on the refinement of the grains upon cooling from the β region or the α+β region and subsequent low-temperature ageing to decompose martensite formed upon quenching [4, 29]. There are some commonly used heat treatments for Ti-6Al-4V. Typical descriptions of the temperatures and times for each treatment are provided, although actual practices vary among alloy producers and users. Figure 2.5 and Figure 2.6 show microstructures formed from the Ti-6Al-4V alloy as a function of solution temperature and cooling rate. Figure 2.5 shows the microstructures of Ti-6Al-4V in a water-quenched, air cooled and furnace-cooled state from above β-transus temperature and from above martensitic start temperature. Martensite appeared in the case of water quench condition but it was absent in air cooled and furnace cooled condition [3].

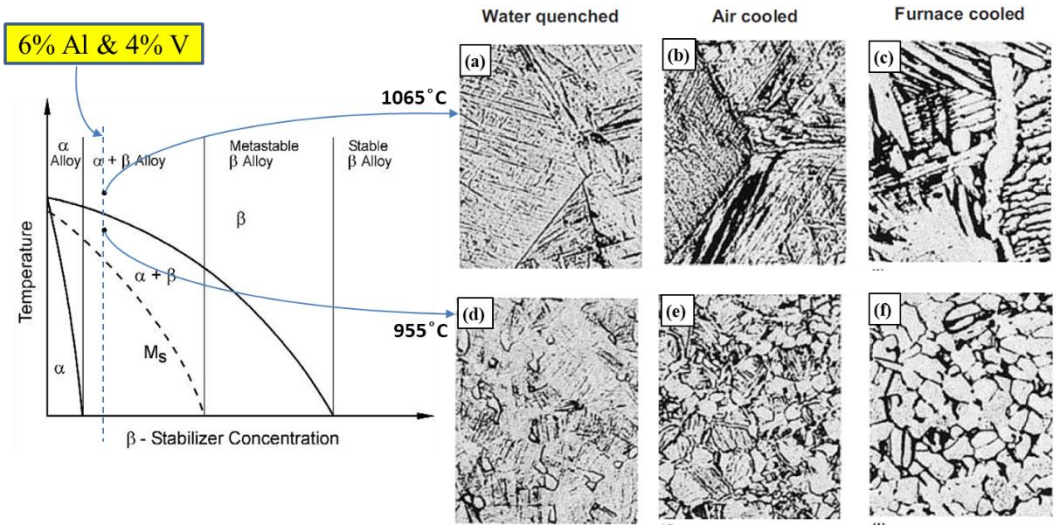

Figure 2.5 (a) α' + β and prior-β grain boundaries; (b) acicular α + β and prior-β grain boundaries (c) plate-like α + β and prior-β grain boundaries; (d) primary α and α' + β; (e) primary α and acicular α + β; (f) equiaxed α and intergranular β [3]

Figure 2.6 shows the microstructures of Ti-6Al-4V in water-quenched, air-cooled, and furnace-cooled states from the (α+β) region, below the martensite start temperature and below the martensite finish temperature [3]. Similar to the above case, martensite appeared in the water quench condition when cooled from above the martensite finish temperature. No martensite appeared in any of the cases when cooled from below the martensite finish temperature; only variations in microstructure were observed [3, 29].

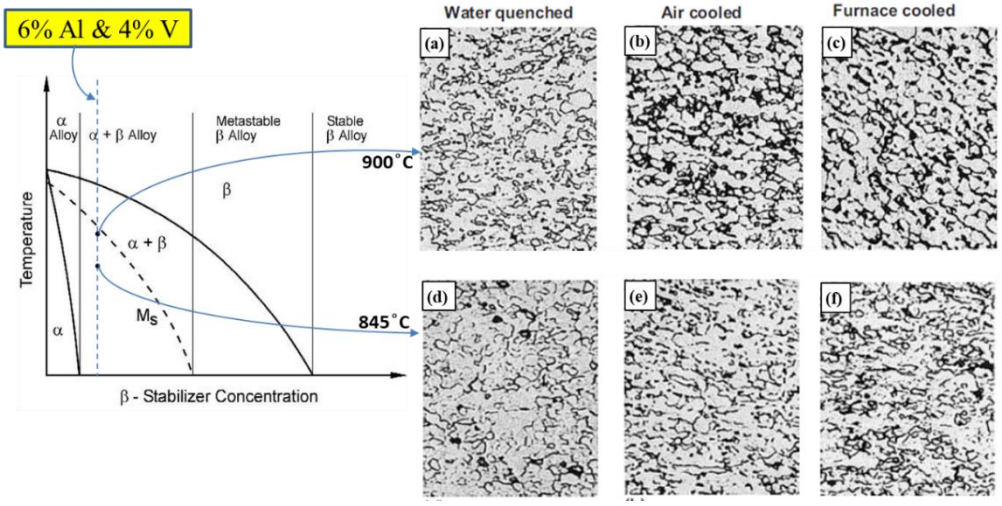

Figure 2.6 (a) Primary α and α' + β; (b) primary α and acicular α + β; (c) equiaxed α and intergranular β; (d) primary α and metastable β; (e) primary α and β; (f) equiaxed α and intergranular β [3]

There are also some annealing treatments used to modify the microstructure and alter the mechanical properties. The first annealing treatment is performed to keep the alloy in a soft, relatively machinable condition. The alloy is heated to about 730°C in the lower range of the (α+β) region, held for 4 hours, and then furnace cooled to 25°C. This treatment, called mill annealing, produces a microstructure of globular crystals of beta in an alpha matrix (refer to Figure 2.2 (b)) [3]. Another annealing treatment is duplex annealing, with several variants used. Typically, the alloy is heated to 955°C for 10 minutes, then air-cooled. It is then heated to 675°C for 4 hours and air-cooled to 25°C. With the aging treatment called solution treating and aging, typically the alloy is heated to 955°C for 10 minutes, water-quenched, then aged for 4 hours at a temperature between 540 and 675°C, followed by air cooling to 25°C. The mill-annealed condition is stronger than the duplex-annealed condition, but the difference is slight. Equiaxed microstructures are obtained by extensive mechanical working of the material in the (α+β) phase field, breaking up the lamellar alpha [5].

2.1.5 Effect of microstructure development on mechanical properties

The microstructure of a material significantly impacts its mechanical properties. Finer grains, achieved through processes like rapid cooling or mechanical working, generally increase a material's strength and hardness but have relatively low ductility and toughness due to the grain boundary strengthening effect, as described by the Hall-Petch relationship. On the other hand, larger grains may improve ductility but decrease strength. The presence and morphology of different phases (such as martensite) can affect toughness and wear resistance. Ultimately, altering the microstructure through processing techniques like heat treatment and welding greatly affects the material's mechanical properties. A few common types of microstructures

and their effects on mechanical properties have been listed in Table 2.3 [34]. A coarser structure of Widmanstätten α and retained β, or a mixture of this structure and α', is produced, which exhibits yield and tensile strengths superior to those of the mill-annealed base metal and ductility and toughness greater than those of an entirely martensitic microstructure. The bimodal microstructure takes advantage of both equiaxed and lamellar microstructures [2].

Table 2.3 Different types of microstructures and their effect on mechanical properties [34]

Fine grains	**Coarse grains**
• High strength • Low ductility • Reduced crack propagation (prerequisite for super plastic deformation) • High fatigue strength	• Creep resistance increases • Fatigue crack growth increases
Equiaxed	**Lamellar**
• High ductility • High strength • Preferred for super plasticity	• High fracture toughness • Superior resistance to creep and fatigue crack growth

2.2 Early development in welding of titanium alloys

Titanium alloys used in aerospace structures require high-integrity joints to meet design requirements. Gas tungsten arc welding (GTAW), laser beam welding (LBW), and electron beam welding (EBW) are all processes capable of creating fusion joints [24, 35]. These processes, however, required precise control of welding parameters and shielding arrangements to prevent atmospheric contamination and ensure sound welds [36]. Among other welding processes, GTAW offers the potential to achieve welds of equal quality to EBW or LBW at much lower capital costs [8]. Over time, researchers developed advancements such as improved shielding gases, shielding arrangements, welding equipment, and filler materials to

enhance the weldability of titanium alloys. Innovations like plasma arc welding (PAW), friction stir welding (FSW) and pulsed gas tungsten arc welding (pulsed-GTAW) further expanded the welding options for titanium alloys, offering improved control, efficiency, and joint quality [14]. The application of pulsed-GTAW involves gaining an understanding of the complex process characteristics. These developments paved the way for the widespread use of titanium alloys in critical applications across the aerospace, medical, and automotive industries, highlighting the continuous evolution and importance of welding technologies in material fabrication[8, 37-39].

2.2.1 Solid-state welding of titanium alloys

Solid-state welding techniques such as friction welding, diffusion welding, and friction stir welding are also gaining popularity for welding titanium alloys, particularly dissimilar titanium alloy welding. *Zhao and Fu (2014)* performed dissimilar linear friction welding on TC11 (Ti-6.5Al-3.5Mo-1.5Zr-0.3Si) and TC17 (Ti-4Mo-4Cr-5Al-2Sn-2Zr) titanium alloys and studied the stain hardening behaviour and fracture characteristics of the welds [40]. The authors observed that the strain rate sensitivity of the welding joint decreased with increasing plastic strain, and the fracture location was between the TC11 and TC17 joints, almost in the region with lower hardness. *Wang et al. (2014)* explored solid-state ultrasonic spot welding for joining Al/Ti alloys and studied the microstructural and mechanical properties of the weld [41]. They observed completely different microstructures in the interface region, and no sample failed at the interface. Diffusion bonding is a common welding method for joining dissimilar titanium alloys or titanium alloys with other alloys, either with or without an interlayer. *Tuppen et al. (2005)* prepared a diffusion bond between the dissimilar Ti-6Al-4V and Ti 550 titanium alloys at laboratory scale, and

the mechanical performance of the bonds was assessed under monotonic tensile and low cycle fatigue [42]. They observed that performance was occasionally influenced by the presence of a bond line defect. Among all the solid-state welding processes for titanium alloys, friction stir welding (FSW) shows very promising results and can be used for industrial applications. Although a few works have been reported on FSW of pure titanium, most of the work reported is directed towards the welding of the Ti-6Al-4V alloy. *Lee et al. (2005)* studied the microstructural evolution of commercially pure titanium using a tungsten carbide tool [43]. The authors observed the grain growth from the weld nugget (WN) to heat affected zone (HAZ). *Knipling and Fonda (2009, 2010)* studied the texture evolution in friction stir welds of near-alpha titanium alloys [44, 45]. They concluded that welds consisted of small, equiaxed prior-β grains delineated by grain boundary α and containing α-laths. There have also been some additional studies on the evolution of the microstructure, micro-texture, and mechanical properties of pure titanium [46-49]. Most of these studies concluded that deformation induced finely recrystallized grains in nugget zone during FSW. The dislocation density was found to increase during friction stir welding, resulting in mechanical properties better than those predicted by the Hall-Petch relationship. *Ramirez and Juhas (2003)* conducted a study on friction stir welding of Ti-6Al-4V, where they observed cooling rate during FSW was slow enough from to cause formation of grain boundary α along the prior β grain boundaries but rapid enough to cause stacking fault formation on basal planes in the α phase [50]. Other research on friction stir welding of Ti-6Al-4V studied the development of grain structure [51, 52], residual stress [53], superplasticity [54], etc. FSW, resulting in lamellar (α+β) microstructure in the stir zone. It was also concluded that the size of α in the microstructure and mechanical properties changes with process parameters [55-57].

Most of these studies concluded that the hardness and strength of the weld were lower than those of the base material, with failures occurring in the lower hardness region. These results indicate that solid-state processes require further exploration of process parameters before they can be considered a viable welding option for aerospace titanium welds.

2.2.2 Fusion welding of titanium alloys

Commonly, titanium alloys are welded using expensive processes such as electron beam welding (EBW), laser beam welding (LBW) etc., to reduce distortion and save from atmospheric contamination [36, 58, 59]. Apart from high cost, these high energy beam processes have several drawbacks, like high hardness in the weld and HAZ, low impact toughness, large micropores, and decreased corrosion resistance [6, 60]. The gas tungsten arc welding (GTAW) can prove to be the best welding process for titanium alloys, if its parameters are optimized, and weldment could be protected from atmospheric contamination. Titanium welds produced using GTAW process have comparable mechanical properties to the welds obtained using EBW process at reduced cost, which stimulated the attention of welding community to use the GTAW process for welding of titanium alloys [35]. Besides the above challenges, excessive grain growth in the weld and heat affected zone (HAZ), and weld distortion due to thermal stresses, particularly with high heat input sources, are also significant [23, 61] Therefore, adequate shielding and optimal heat input are essential for welding titanium alloys. A variant of GTAW known as pulsed-GTAW attracted the researchers as a potential welding process for precision welding of titanium alloys and used for very demanding applications like cryogenic bellows, nuclear power plant pipe work and welding of aircraft gas turbine and their components [14, 62]. Pulsed-GTAW includes the stable arc, ductile welds, and excellent control over heat input which

helps in obtaining improved weld penetration, reduced distortion, reduced thermal build-up, and good weld aesthetic welds [14, 63]. Current pulsing during welding helps in achieving compressive residual stress or reduced tensile residual stress intensity compared to the conventional GTAW process [64]. In addition to these advantages, current pulsing during welding also facilitates grain refinement in the HAZ and weld zone, and refines the laths of α in the Widmanstätten morphology of the HAZ and weld zone [61]. Most of these advantages could not be obtained with conventional GTAW process [14].

2.3 Classification of typical GTAW weldment

Conventional GTAW is a low-power density and low arc pressure welding process where heat is predominantly conducted through the base metal. As the temperature of the base metal is raised, it melts and forms a wide and shallow weldpool, as shown in Figure 2.7. The different regions of the weldment, including the heat affected zone (HAZ), solidified weld metal (weld region), and melting region, are labelled in the figure. This is sometimes referred to as a conduction-mode weld pool. Often, this type of weld pool is desired for joining thin sections, as these parts tend to be difficult to form accurately. The conduction-mode weld pool is intrinsically stable because vaporization of the base metal is negligible [65]. Because of the stability and simplicity of conventional-GTAW equipment, it is also used for manual welding. However, the maximum thickness that may be welded by conventional GTAW is limited, and joint preparation is required for butt joint thicknesses greater than 2-5 mm [66].

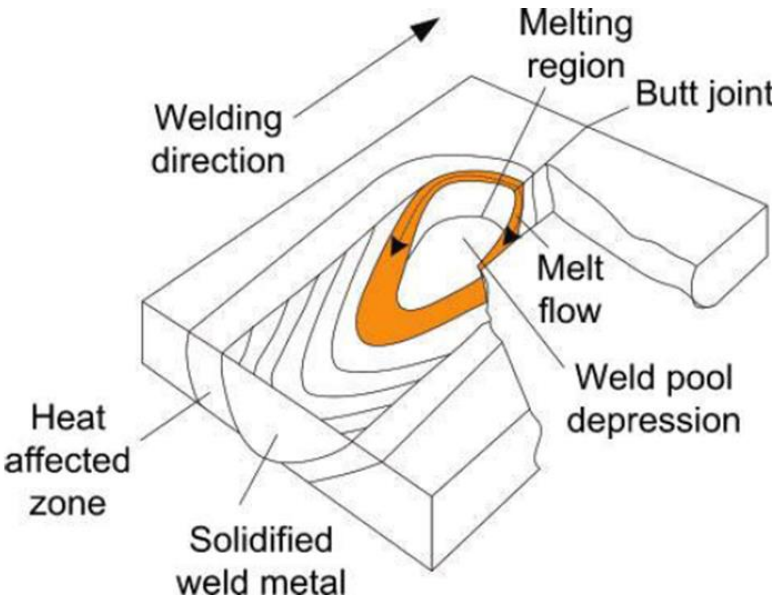

Figure 2.7 Schematic of conduction mode weldment [8]

2.3.1 Typical gas tungsten arc welded Ti-6Al-4V alloy weldment

The cooling rate in welding is generally fast compared to casting, leading to non-equilibrium solidification in the weld region. Figure 2.8 illustrates a typical weldment from gas metal arc welding (GTAW) of Ti-6Al-4V, showing a wide and shallow weld pool post-welding. The fusion boundary is highlighted, delineated by the arrowhead ending on the fusion boundary. Solidification during the welding of titanium alloys follows epitaxial grain growth, where solidification occurs following the previous half-melted grain in the heat-affected zone (HAZ). Sometimes, the fusion boundary is not revealed with simple etching, so macro-etching using concentrated acid or numerical models is used to determine the maximum temperature reached and correlate different regions. Isotherms generated from a numerical model depict different regions, like the fusion zone (FZ), HAZ, and base region, indicating the maximum temperature in each area. This comprehensive analysis calculates heat transport by assessing the relative importance of convection and conduction [8, 67].

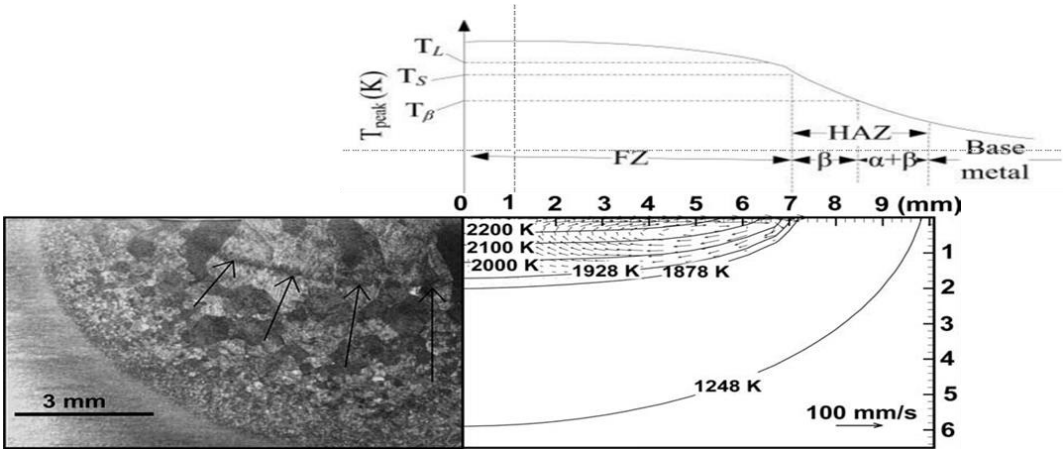

Figure 2.8 A typical gas tungsten arc weld geometries in Ti-6Al-4V and comparison with temperature ranges obtained from numerical model [8, 67]

2.3.2 Microstructures in different regions of Ti-6Al-4V weldment

Fusion zone: ($T_{max} > T_L$)

1. The temperature in this region is above liquidus temperature (T_L).
2. The development of fusion zone (FZ) microstructure is significantly influences by the base metal microstructure, as growth of prior-β grains take place epitaxially.
3. The prior-β grain size increases with specific heat input during welding.
4. The fusion grain boundary is not easily distinguishable due to the epitaxial growth and severe grain coarsening in FZ and HAZ.
5. The embrittlement due to atmospheric contamination and porosity due to improper cleaning are the two major weld defects.
6. In thin sections (< 2 mm), the prior-β grains in FZ may cross the complete joint thickness.

Near HAZ: (T_{max} b/w T_b and T_L)

1. This is the region of HAZ adjacent to fusion boundary.

2. The temperature in this region lies between β-transus temperature (T_b) and liquidus temperature (T_L).
3. Severe grain coarsening of prior-β grains take place in this region.
4. Depending upon the cooling rates different type of microstructure is obtained in this region.

Far HAZ: ($T_{max} < T_b$)

1. This is region HAZ adjacent to the base metal and away from the fusion boundary.
2. The temperature in this region is below T_b and sufficient for microstructural change.
3. This temperature in region is difficult to define as it depends on transformation kinetics.

Base metal or unaffected region

1. This is region far away from the fusion zone.
2. The microstructure of this region is unaffected due to heat supplied during welding.
3. Very rare or no mechanical properties affected in this region.

2.4 Major challenges during welding of titanium alloys

There are various challenges that arise during the welding of titanium alloys, as discussed in Section 1.4. A few of the challenges, like ferrite contamination and porosity, could be avoided by taking various precautions and following proper cleaning procedures. However, there are still a few challenges that need proper attention during the welding of titanium alloys, such as embrittlement due to atmospheric contamination and severe grain coarsening in HAZ and the fusion zone.

A detailed literature review has been done for the shielding arrangements used to avoid atmospheric contamination and how current pulsing helps GTAW in grain refinement.

2.4.1 Shielding arrangement from atmospheric contamination

As discussed previously, atmospheric contamination is very severe during the welding of titanium alloys because they absorb oxygen, nitrogen, and hydrogen even at a temperature as low as 427 °C. Excessive absorption of these gases causes embrittlement in the weld and nearby region [3]. Visually, the contamination level can be assessed on the basis of the colour that appeared on the top and root sides of the weldment. For example, a bright silvery colour on the top and root sides of the weldments is considered atmospheric contamination free and the weld is considered acceptable. Discolorations like blue, gray, and white reveal improper shielding during the welding of titanium and the weld is rejected [16, 68]. The colour of the weld bead varies depending on the thickness of the oxide layer, where the chalky white colour of the weld bead is considered highly atmospherically contaminated and therefore rejected. The list of colours that appeared on the titanium alloy weld, along with their acceptance and rejection, is listed in Table 2.4 [22]. There are various shielding arrangements made to protect the weldment from atmospheric contamination. A few shielding arrangements by various researchers have been discussed.

Table 2.4 Acceptable/ unacceptable weld bead colour in titanium welding [22]

Weld bead colour in welding of Titanium	**Acceptable/ Unacceptable**
Bright silver	Acceptable
Silver	Acceptable
Straw	Acceptable
Violet	Unacceptable
Blue	Unacceptable
Green	Unacceptable
Gray	Unacceptable
white	Unacceptable

Welding titanium alloys in a vacuum chamber or in an inert atmosphere could avoid the problem of atmospheric contamination. The atmospheric contamination can be avoided using box shielding, trailing cups, back purging, a high gas flow rate, and the lamellar flow of shielding gases on the weldment [3]. *Karpagaraj et al. (2015)* produced sound welds using GTAW with shielding gas flow of 15 l/min through primary shielding, 25 l/min through trailing cup, and 10 l/min through bottom or back purging, i.e., total 50 l/min flow rate of shielding gas was used [22]. *Bendikiene et al. (2018)* produced welds by creating an argon gas-filled box shielding arrangement where they used shielding gas flow rates of 10 l/min from the torch, 20 l/min from the track tool, and 27 l/min from the back tool, i.e., a total 57 l/min of shielding gas flow rate was used for obtaining a sound weld [69]. Similarly, *Gao et al. (2022)* also used back purging and trial shielding to produce a sound weld using electron beam welding (EBW) [58]. There are also few shielding arrangements commercially available for welding other than flat butt welds like pipe welds, corner welds and tube welds as shown in Figure 2.9 [70].

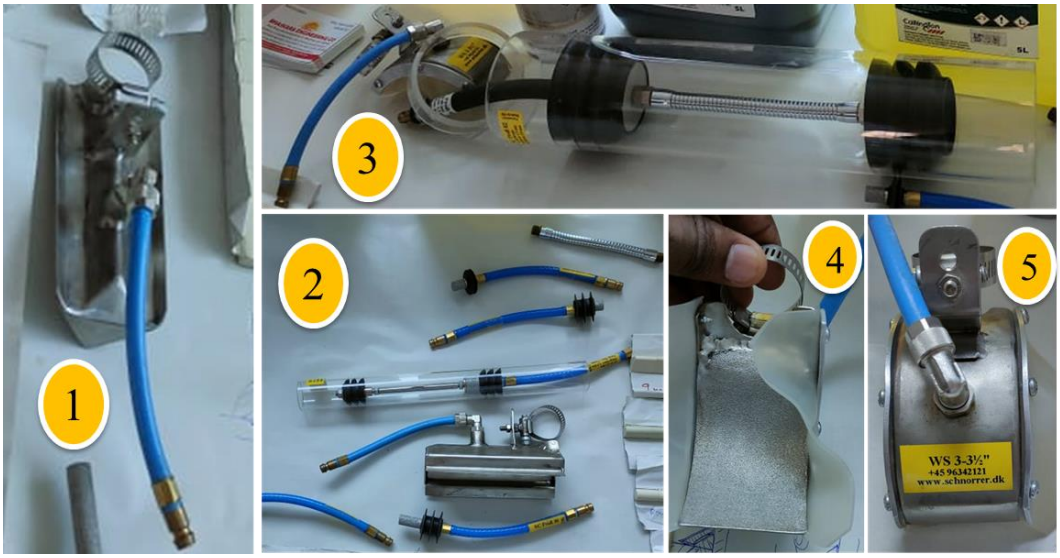

Figure 2.9 Commercially available shielding arrangements: (1, 2) trailing shield; (3) vacuum chamber for pipe weld; (4, 5) bottom and top of trailing shield [70]

2.4.2 Effect of current pulsing during GTAW on titanium alloys welds

Current pulsing during GTAW is an approach for the refinement of prior-β grains and morphology in the weld and HAZ of titanium alloys. Several studies related to refinement in the microstructure of welds and HAZ of (α+β) titanium alloys using pulsed-GTAW have been discussed. *Sundaresan et al. (1999)* performed a macrostructural examination of Ti-6Al-4V alloy welds prepared using pulsed and unpulsed current conditions during GTAW [23]. Both the welds were prepared at 105 A mean current to maintain the same heat input. Grain refinement was observed using pulsed current due to the enhancement of fluid flow, which reduces temperature gradients and causes a continual change in the weld pool size and shape. The macrostructural examination of the weld also showed that the minimum grain size was observed at a pulse frequency of 6 Hz. *Babu et al. (2006)* studied the influence of current pulsing on the microstructure and mechanical properties of Ti-6Al-4V TIG weldments [71]. Unpulsed parameters were 120 A arc current, 10 V arc voltage, and pulsed parameters were 330 A peak current, 66 A background current, 11 V arc voltage, and 6 Hz frequency. It was reported that the pulsing of welding

current resulted in grain refinement in α-β titanium alloy welds. This was attributed to the greater physical disturbance in the weld pool caused by current pulsing. The reduction in prior-β grain size improved the strength and ductility of pulsed current weldments in comparison to unpulsed current welded specimens. *Balasubramanian et al. (2008)* investigated the effect of pulsed current Gas Tungsten Arc (GTA) welding parameters on the corrosion behaviour of the Ti-6Al-4V titanium alloy [72]. The investigation revealed that corrosion resistance increased with higher peak current and pulse frequency up to an optimal value, beyond which corrosion resistance decreased. Additionally, an increase in corrosion resistance with grain refinement was also detected. *Balasubramanian et al. (2009)* developed a mathematical model to predict the grain size and hardness of pulse current tungsten arc welded Ti-6Al-4V titanium alloy. The authors welded the 1.6 mm thick Ti-6Al-4V sheets using pulse current tungsten arc welding (PC-GTAW) with a peak current range of 60-100 A and a base current 20-60 A in a frequency range of 0-12 Hz with a varying peak current time percentage. The refinement in prior-β grains was observed using PC-GTAW, and the arc became unstable above the 6 Hz frequency [73]. *Mehdi et al. (2016)* compared the microstructure and residual stresses in Ti-6Al-4V alloy welds prepared using unpulsed (conventional) and pulsed TIG welds at 1 and 5 Hz frequencies [64]. The authors prepared unpulsed welds at 80 A and 10 V, and pulsed parameters were 100 A peak current (I_p), 50 A (50 % I_p), background current, 100 mm/min welding speed, and 50%-time peak current. Increasing the pulse frequency during pulsed TIG welding refines the prior-β grain size in the fusion zone and HAZ of the Ti-6Al-4V alloy compared to the unpulsed process. Current pulsing at 5 Hz also helped in obtaining lower tensile residual stresses in the weld region in comparison to the weld produced using unpulsed TIG. Current pulsing not only

helped in grain refinement but also helped in obtaining improved hardness, improved tensile strength, reduced distortion, and improved bead contour [61, 74].

2.4.3 Effect of electrode tip angle weld geometry

In addition to the key welding parameters (welding current, welding speed, and arc voltage), the electrode tip angle also plays an important role in the weld bead geometry during GTAW [75-77]. *Goodarzi et al. (1997)* observed during GTAW that electrode tip angle alters weld pool shape and size and other features of the weld by modifying the gas shear stress and energy density (heat flux) of the arc [78]. An increase in electrode tip angle led to an increase in the energy density found at the anode and a decrease in the convective contribution of heat flux at the anode due to a reduction in gas velocity. The highest heat flux was observed in the range of 30° to 60° electrode tip angle during GTAW. The weld pool becomes unstable at extremely low electrode tip angles due to an increase in arc pressure and a decrease in arc length [14]. The variation in optimum electrode tip angle was observed in variants of GTAW. *Ukita et al. (2002)* analyzed the effect of electrode tip shape and torch angle during GTAW of thin aluminium sheets [79]. They suggested that the combination of a 30° cone angle with 25 % spherical surface area and a 15° backward inclination of the torch helped in performing effective ultra-high-speed welding of ultra-thin aluminium sheets. *Hsuan et al. (2012)* observed during A-GTAW, electrode tip angle played a major role in weld bead profile and that the optimum electrode ranged from 60° to 75° [80]. Along with the electrode tip shape, the processing of tungsten electrodes also needs a lot of attention, like cleanliness, processing direction, and safety [14, 19].

2.5 Dissimilar welding of titanium alloys

The requirements and complexities that occur during dissimilar welding of titanium alloys have been discussed in Section 1.5 and its sub-section. Although the dissimilar welding of titanium alloys is affordable using the GTAW process, at the same time, it is very difficult to obtain a tailored weld using it. There are several studies that have been performed on dissimilar welding of titanium alloys, but only a few studies have been performed using GTAW or its variant. *Zhang et al. (2006)* performed dissimilar welding of Ti3Al and TC4 using the EBW process and studied the interfacial microstructure and strength of the joint [81]. The grain coarsening was observed with increasing heat input, and the highest tensile strength of the joint was near the strength of the base of the Ti3Al alloy with 8 % reduction. *Tan et al. (2010)* used the EBW process to weld Ti-22Al-25Nb and TC11 alloys, and martensite (α') was observed in the HAZ region and a large quantity of O/α2 particle precipitate in the weld region [82]. Reduced impact strength and comparable tensile strength to the TC11 were observed in the weld region of the weld. *Wang et al. (2014)* created dissimilar joints of Ti-6Al-4V and Ti17 alloys using the EBW process and studied the influence of strain rate and temperature on the tensile properties, strain hardening behaviour, strain rate sensitivity, and fracture characteristics of the dissimilar welds [83]. The increase in strain rate or decrease in temperature, increased the strain hardening rate at a given true stress. The welded joints failed in the Ti-6Al-4V base metal near the HAZ, and the fracture surfaces exhibited dimple fracture characteristics at different temperatures. *Hsieh et al. (2016)* used CO2 laser for dissimilar welding of Ti-15V-3Cr-3Al-3Sn to Ti-6Al-4V titanium alloys and compared the microstructure and tensile strength variation in as-weld and post-weld heat treatment (PWHT) conditions [84]. High hardness in the weld region was

susceptible to the PWHT, the spikes in hardness in the as-weld condition converted into plateau after PWHT. *Cheng et al. (2018)* performed dissimilar welding of TC17 and Ti60 using EBW and investigated the microhardness and tensile properties of the dissimilar joints [85]. Rod-like α and β phases appeared in the fusion zone (FZ), equiaxed α phases, fine α laths and β phases in the heat-affected zone (HAZ) of the TC17 side and acicular martensite α' phases and retained α phases in the HAZ of the Ti60 side. Homogeneity in the hardness was observed across the weldment, and all tensile-tested specimens fractured from the low-strength Ti60 side. There are several similar studies that were performed on the dissimilar welding of titanium alloys using GTAW or other welding processes. These studies include dissimilar welding of Ti-22Al-25Nb/TA15 using LBW [86] and Ti-6Al-4V/Ti-6.5Al-3.5Mo-1.5Zr-0.3Si using EBW [87].

2.5.1 Dissimilar welding of CP-Ti and Ti-6Al-4V

Although CP-Ti possesses excellent formability, higher corrosion resistance, good impact toughness, good stress corrosion cracking, and is cheaper than other titanium alloys, its strength is lower than other alloys of titanium. On the other hand, Ti-6Al-4V has excellent strength, good corrosion resistance, but reduced formability [3]. These two alloys, when used together, can provide the advantages of both high strength and formability. Therefore, the investigation of dissimilar welding of CP-Ti to Ti-6Al-4V is vital to meet various industrial requirements.

Dissimilar welding of commercially pure titanium (CP-Ti) and Ti-6Al-4V alloy together presents challenges due to their differing compositions and properties. CP-Ti consists mainly of titanium with low interstitial elements, making it relatively soft and ductile compared to Ti-6Al-4V, which contains alloying elements like aluminium and vanadium for enhanced strength and hardness [5]. These two alloys, when used

together, can provide the advantages of both high strength and ductility. Therefore, the investigation of dissimilar welding of CP-Ti to Ti-6Al-4V is vital to meet various industrial requirements [68]. Furthermore, dissimilar welding of CP-Ti and Ti-6Al-4V requires meticulous joint preparation, including surface cleaning, proper fit-up, and tack welding, to minimize contamination and ensure good fusion between the dissimilar materials. Post-weld heat treatment (PWHT) or stress-relief processes may also be necessary to alleviate residual stresses and improve the overall performance of the welded joint [18].

Casalova et al. (2011) performed dissimilar welding of grade 2 (CP-Ti) and grade 5 (Ti-6Al-4V) using laser and hybrid welding, and studied the joint fatigue strength [88]. The authors observed that the fatigue strength reduction factor for a titanium hybrid welded joint increased linearly with respect to the logarithm of the number of cycles to failure. *Adamus et al. (2013)* welded the 0.8 mm thick sheets of CP-Ti and Ti-6Al-4V by EBW using 4 mA beam current and 50 kV accelerating voltage and performed numerical analysis for aerospace applications [89]. *Lin et al. (2017)* also welded 1 mm thick sheets of CP-Ti and Ti-6Al-4V for aerospace and nuclear applications using EBW and performed stretch forming tests to study the formability of dissimilar joints [90]. *Froend et al. (2017)* used a continuous-wave 8kW ytterbium fiber laser for welding of CP-Ti (skin) and Ti-6Al-4V (stringer) and produced T-joints for aerospace applications [68]. *Logesh et al. (2020)* performed LBW of grade 2 (CP-Ti) and Ti-6Al-4V and investigated the effect of severe double shot peeing on weldment. α/α′ phases were observed in the HAZ, and fractography of tensile samples revealed the inner minor cracks and voids at the fusion zone [91]. *Kim et al. (2023)* studied the microstructure and mechanical properties of dissimilar friction-welded CP-Ti and Ti-6Al-4V alloys [92]. The yield and tensile strengths of welded

specimens were maintained at a similar level to those of CP-Ti-2, and the tensile specimens were fractured at the base material zone of CP-Ti-2, not at the weld interface and its periphery. *Zahabi et al. (2024)* welded CP-Ti and Ti-6Al-4V using spark plasma welding and studied the microstructural and mechanical properties [93]. The alloy (CP-Ti/Ti-6Al-4V), bonded at 800 °C for 10 minutes under a pressure of 20 MPa, exhibited superior bonding with an interface thickness of 7-9 μm, excellent tensile strength (534 ± 13 MPa), and Vickers micro-hardness (190 ± 5 HV0.1). There are several similar studies that were performed on the dissimilar welding of CP-Ti and Ti-6Al-4V alloys using different welding processes [94-96].

2.6 Impression creep testing of titanium welds

The weldment mostly consists of three distinct zones known as weld zone, heat affected zone (HAZ), and base metal. Most alloys including titanium alloys possess different mechanical properties such as hardness, tensile and creep strength in the different regions of the weldment, due to the appearance of different microstructures in each zone [1, 3]. The independent investigation of creep properties is essential in different zones of the weldment before putting them in service. Due to the very narrow zone with limited testing area, conventional creep testing methods would be extremely difficult to obtain zone-wise creep behaviour of weldments. In order to address this issue, Impression creep testing could be employed for understanding the steady state creep behaviour, determining the activation energy, and determining the governing creep mechanism from the stress exponent. The distinct zones of weldment can be crept separately by placing the indenter in the respective zones of interest. In this method, generally a 1 mm diameter cylindrical indenter made of tungsten carbide is used for localized deformation. The information generated during

the deformation process can be used for analysing the zone wise creep behaviour of weldments [97].

The concept of impression creep testing was derived from the hot hardness testing of the materials, where indentations were made using a spherical, pyramidal, or conical shape indenter at a constant load. *Sherby et al. (1971)* utilized this technique for evaluating the activation energy for creep or self-diffusion in pure metals, including titanium [98]. *Muhammad et al. (2022)* studied the impression creep behaviour of different regions of pulsed-gas tungsten arc welded Ti-5Al-2.5Sn alloy using nano-indentation and atomic force microscopy [99]. But the hot hardness technique used by these authors was not justified for the creep studies since the hardness of the material decreased with testing time and the magnitude of stresses also decreased due to the shape and size effect of the indenter [100]. Hardness decreasees with testing time in Ti-6Al-4V as well, in order to overcome this shortcoming of the hot hardness test, *Chu et al. (1977)* utilized cylindrical indenter with a flat end to achieve steady state velocity in the secondary stage of creep deformation [100]. The technique was named as ‘impression creep testing’. This technique is suitable for evaluating the steady state creep behaviour of narrow regions. However, the study of tertiary creep behaviour is not possible using this technique due to the fact that the material is subjected to compressive stresses, and rupture does not happen with such small strains accommodated during impression creep testing. Depending upon the area available for testing, impression creep testing can be performed using a 0.5 mm, 1 mm, or 2 mm diameter cylindrical indenter [101]. *Yu et al. (1984)* performed impression creep testing on Ti-6211 alloy in the stress range of 1500-5661 MPa at room temperature, and exhaustive type creep behaviour was analysed at stresses less than 3000 MPa [102]. *Surya et al. (2019)* utilised the impression creep testing to

investigate the zone-wise creep behaviour of SMAW, TIG, and A-TIG welded 9Cr-1Mo steel [103]. *Eftekhar et al. (2021)* also performed impression creep testing on different zones of TIG-welded semisolid casted AXE622 Mg alloy, they observed power law breakdown as the controlling creep mechanism in the base metal and dislocation creep mechanism in the HAZ and weld zone in their investigation [104]. Several other studies were also performed on different microstructural regions of welded as well as casted specimens [105-107].

The weldments of any mechanical component used for high-temperature applications are always very critical due to its distinct zones with varying microstructure, making it prone to failure [108]. For example, the high-pressure and low-pressure compressor blades, casing and other parts of gas turbines for aerospace applications are made of Ti-6Al-4V alloy, which are exposed elevated temperatures at high stresses during their service periods [2, 109]. Hence, the analysis of the creep behaviour of the different zones of weldment is very essential to get insights about the microstructural degradation mechanisms and predict the service life of a component. *Harrigan et al. (1974)* performed creep testing on repair welded Ti-6Al-4V castings at 315 °C and 650 °C with a range of stresses from 138 MPa to 620 MPa [110]. They reported that creep strength of Ti-6Al-4V alloy castings has improved significantly after weld repair. *Pederson et al. (2012)* performed the conventional creep test on dissimilar titanium (Ti64/Ti6246) welds, where they reported that the failure took place in the heat affected zone (HAZ), at a location away from the weld [111].

2.7 Research gaps

1. The demand for dissimilar welding is increasing because modern industries require innovative, high-performance, and cost-effective products and

structures that take advantage of the strengths of different materials while addressing specific design and functional requirements.

2. Affordable, defect-free welding of titanium alloys is still a challenge due to their high reactivity with atmospheric gases and severe grain growth in the HAZ and weld region caused by low thermal conductivity.
3. High hardness, reduced toughness, and large micropores appear in the weld region of titanium alloy weldments produced using high-energy beam welding processes, which are commonly used for welding titanium alloys.
4. Gas tungsten arc welding (GTAW) and its variants exist as affordable welding processes for titanium alloys. They can prove to be the best welding process for titanium alloys if their parameters are optimized and the weldment is protected from atmospheric contamination.
5. Dissimilar welding of commercially pure titanium (CP-Ti) and Ti-6Al-4V alloy is in demand for aerospace and nuclear applications due to the requirement for different mechanical properties in different components.
6. Very limited literature is available on dissimilar titanium welding, specifically the dissimilar welding of CP-Ti and Ti-6Al-4V alloy using cost-effective conventional GTAW and pulsed GTAW.
7. Limited literature is available on the effect of different pulse and process parameters used during gas tungsten arc welding and the selection of process parameters for dissimilar welds.
8. No literature is available on impression creep testing of different zones in dissimilar titanium weldments produced using pulsed GTAW for high-temperature applications of titanium alloys.

2.8 Objectives for the research

1. Develop a method for successful and defect-free dissimilar welding of commercially pure titanium (CP-Ti) and Ti-6Al-4V alloy using cost-effective conventional and pulsed GTAW processes.
2. Develop an affordable shielding setup for protecting the weldment from atmospheric contamination during welding without using any external shielding such as back purging, trailing shielding, or an inert chamber.
3. Development of dissimilar welds with no hardness spikes throughout the weld, sufficiently good toughness, and free from micropores in the welds.
4. Optimization/selection of pulsed parameters for GTAW to develop the weldment with minimum heat input, reduced weld seam width, better penetration, improved bead contour, and grain refinement in the HAZ and weld region to improve the mechanical properties of that region.
5. Finalization of process parameters for the dissimilar (CP-Ti/Ti-6Al-4V) welding of titanium alloys. These process parameters include peak current (I_p), background current (I_b), time for peak current (T_p), time for background current (T_b), pulsed frequency (f), welding speed, stand-off distance, and electrode tip angle.
6. Analyse and compare the defect-free dissimilar welds produced using conventional GTAW and pulsed GTAW with respect to their microstructure development, mechanical properties, and phase development in each case.
7. Study the high-temperature deformation behaviour of different regions (base metal, HAZ, and weld zone) of the weldment at application temperatures and stresses using impression creep testing.